SAND2016-1870J

Dynamics of Polydots, Soft Luminescent Polymeric Nanoparticles

Sabina Maskey,[1] Naresh C. Osti,[1†] Gary S. Grest[2*] and Dvora Perahia[1*]

[1]Department of Chemistry, Clemson University, Clemson, South Carolina 29634, USA

[2]Sandia National Laboratories, Albuquerque, New Mexico 87185, USA

Abstract:

The conformation and dynamics of luminescent polymers collapsed into nanoparticles or polydots were studied using fully atomistic molecular dynamics (MD) simulations, providing a first insight into their internal dynamics. Controlling the conformation and dynamics of confined polymers is essential for realization of the full potential of polydots in nano medicine and biotechnology. Specifically the shape and internal dynamics of polydots that consist of highly rigid dialkyl *para* phenylene ethynylene (PPE) are probed as a function of temperature. At room temperature, the polydots are spherical without any correlations between the aromatic rings on the PPE backbone. With increasing temperature, they expand and become slightly aspherical; however, the polymers remain confined. The coherent dynamic structure factor reveals that the internal motion of the polymer backbone is arrested and the side chains dominate the internal dynamics of the polydots. These new soft nanoparticles retain their overall shape and dynamics over an extended temperature range and their conformation is tunable via their degree of expansion.

1. Introduction

Soft nanoparticles (NPs) or polydots formed by collapsed luminescent polymers are emerging as promising candidates for various bio-applications[1, 2] due to their photostability, high brightness, and low toxicity. Their biocompatibility and biodegradability enable their use in vivo[3-7] as biosensors, drug carriers, and fluorescent probes for detection and imaging.[8-14] The photophysics of polydots depends on the chromophore's chemical structure, chain conformation, the size of the NP, and the degree of correlations between the aromatic rings.[15-17] While polydots find increasing applications, there is limited understanding of the effects of confinement of conjugated polymers into NPs. In contrast to confinement into aggregates in solution, in polydots the molecules are trapped in the nano dimensions with no correlation between the chromophores. Building on our previous study where we demonstrated the ability to prepare polydots computationaly,[18] the structure and stability of polydots as a function of temperature are probed and their internal dynamics is revealed.

Long-lasting, soft polymeric nanoparticles are commonly made by collapsing macromolecules in dilute solutions followed by crosslinking of the confined state.[19, 20] Polydots or luminescent polymeric NPs form a new, fascinating class of NPs that consist of polymers confined to nano length scales without chemical crosslinking, enabling formation of a dynamic luminescent nano cage. These are formed by initially confining the polymers into droplets in a good solvent that is then dispersed into water, which is a poor solvent for the polymers. With the evaporation of the good solvent, the polymers remain confined to nano dimensions without any additional chemical bonds. The confinement without chemical crosslinking offers a potential for tunability.[21-24] The factors that determine the internal structure, stability, and dynamics of these long-lived, soft polymeric nanoparticles, however, have not been resolved. Here using the computational methodology previous derived[18] for assembly of these confined nanoparticles and response to solvents, we probe the temperature stability and dynamics of polydots that consist of confined polymer, dialkyl *para* phenylene ethynylene (PPE), whose chemical structure is shown in Figure 1. The backbone of PPEs consists of numerous chromophores whose conjugation is strongly affected by the respective orientation of the aromatic rings. Only segments where consecutive aromatic rings are confined into a single plane are fully conjugated. The alkyl

substituents that often serve as solvation moieties affect the electronic structure through conformational dynamics and impact assembly. One unique feature of PPEs is there extended conformation in dilute solutions shown both experimentaly[3] and computationaly.[25] While the most stable conformation in dilute solution is extended,[24] polydots in water remain confined over long periods of time.[18] These two entirely different conformations raise intriguing questions regarding the stability of the confined state, and the dynamic proceses that ultimately control the polydots and their photophysics. Here, we probe the dynamics of the confined state as the temperature is varied. Surprisingly, we find that though the polydots expand somewhat with increasing temperature, they remain confined. Also, the backbone remains rigid while the side chains are dynamic.

The paper is organized as follows: we first present the simulation model and methodology followed by the results of the analysis of the static structure of the polydots. The dynamics studies are then presented, followed by conclusions.

2. Model and Methodology

The PPE chains are modeled using the fully atomistic optimized potentials for liquid simulations–all atoms (OPLS–AA) potentials of Jorgensen et al.[26, 27] They are comprised of bonded and non-bonded interactions. The non-bonded interactions are a sum of the standard 12-6 Lennard-Jones (LJ) potential and a Coulomb electrostatic term. For atoms of different species, geometric mixing rules of $\varepsilon_{ij} = (\varepsilon_i * \varepsilon_j)^{1/2}$ and $\sigma_{ij} = (\sigma_i * \sigma_j)^{1/2}$ are used, where ε_{ij} and σ_{ij} are the LJ units of energy and distance between atoms *i* and *j*, respectively. Non-bonded interactions are calculated between all atomic pairs on different molecules, in addition to all pairs on the same molecule separated by three or more bonds. The interaction is reduced by a factor of 2 for atoms separated by three bonds. All LJ interactions were cut off at r_c = 12Å. The electrostatic interactions for atom pairs closer than 12 Å are calculated in real space; those outside this range are calculated in reciprocal (Fourier) space by the particle–particle, particle–mesh (PPPM) algorithm[28] with a precision of 10^{-4}. Bonded interactions include a harmonic term between bonded atoms, a harmonic three-body angle term, and a four-body dihedral interaction. The form of the interaction and all relevant interaction parameters are described in detail in ref. 26,27.

All simulations were performed using the large-scale atomic/molecular massively parallel simulator (LAMMPS) molecular dynamics code.[29] The equations of motion were integrated using the velocity–Verlet algorithm with a time step δt = 1fs. The temperature T, was regulated through weakly coupling the system to a heat bath using a Langevin thermostat[30, 31] with 100 fs damping time. PPE chains of length 240 repeat units were built using the Polymer Builder in Material Studio from Accelrys Inc. using the polymer consistent force field (pcff), as OPLS–AA potentials are not implemented in Material Studio, and converted to OPLS–AA.[25]

For modeling polydots in water, a system of 648,000 atoms was first equilibrated with SPC/E model for water.[32] The SHAKE algorithm was used to constrain the O-H bond length and H-O-H angle.[33, 34] To immerse the polydots in water, a void in the center of the liquid was created by inserting a soft, repulsive, spherical pseudoparticle into the solvent. This process was similar to that by which the polydots were made, but in reverse, whereby a cavity was grown slowly from radius zero to a size capable of accommodating one polydot. The overall system dimensions were allowed to expand at a constant pressure of P = 1 atm through the time of the void growth. When the desired size was reached, the pseudoparticle was removed, leaving a void large enough to accommodate the polydot. The combined system was then equilibrated at constant pressure P = 1 atm for 1ns, after which it was run at constant volume for at least 300 ns at 300 K. This range probes significantly longer times in comparison with our previous simulations of polydots in water, enabling the study of dynamics.[18]

In addition, following the similarities between the behavior of polydots in water and in implicit solvents, simulations were run in implicit poor solvents offering a means to study the behavior of the polydots for longer times, capturing further dynamic information. The quality of implicit solvents was controlled by varying the strength of the attractive interactions between non-bonded atoms.[35] To model a solvent that was poor for both the backbone and side chains, all the LJ non-bonded interactions were truncated at r_c = 1.2 nm. The simulations in an implicit poor solvent were run at temperatures T = 300, 400, and 600 K for at least 300 ns each. While 600K is above the temperature where the bonds would break experimentally, it allows us to study the limit of the stability of the polydot. Polydots equilibrated in an implicit poor solvent at 300 K for 25 ns were also heated to 400 and 600 K. After equilibrating polydots at 400 and 600 K for 150 ns, they were then cooled down to 300 K.

3. Preparation of Polydots

Using a process close to the experimental preparation method, the polydots were formed by compressing an isolated chain to a collapsed state and then letting it relax in a poor solvent.[18] A schematic representation of the preparation is shown in Figure 2. The molecules were enclosed in a large spherical cavity, whose radius was slowly reduced over 1 ns. The cavity wall interacts with the PPE chain via a harmonic potential. PPE as prepared and in its early stages of compression is shown in Figure 2a-d. The polymer molecules were initially compressed to dimensions that resulted in internal density comparable to that of polymer melts. This criterion resulted in a final diameter of 5.0 nm for a diethylhexyl-substituted PPE and 2.0 nm for a bare PPE chain. Once the density of the polydot reached its bulk value, the spherical cavity was removed and the confined state was allowed to relax in water or in an implicit poor solvent. A visualization of a diethylhexyl PPE polydot as prepared is shown in Figure 2e. The polydots equilibrated at 300K retained their spherical shape with a smooth interface dominated by the side chains, after 300 ns, as shown in 2f in an implicit poor solvent and Figure 2g in water. The polydot surface is dominated by the alkyl chains with limited backbone segments residing at the interface.

Our previous results have shown that[18] in an implicit poor solvent and water, polydots remain compact over 100 ns at 300 K, consistent with the experimental findings.[15,16] The polydot immersed in water and in implicit poor solvent assumes the same radius of gyration, density profiles, and static structure factor S(q). These similarities persist for both substituted and bare PPES. Here we probe in greater detail the dynamics of the polydots in water and implicit solvent at 300 K and study the effect of increasing the temperature in an implicit solvent.

4. Results and Discussion

A. Structure Studies.

Snapshots of diethylhexyl PPE polydots and polydots of the bare PPE in an implicit poor solvent are shown in Figure 3 at three temperatures. These polydots are depicted 300 ns after the removal of the constraint at 300 K and 300 ns after heating to higher temperatures. Two different conformations of the polydots, shown in Figures 2e and 2f, were then heated to 400 K and 600 K. Starting from either conformation resulted in a similar final state. Comparing the images in

Figure 3a and Figure 3b, clearly shows that the conformation of the backbone of the polydots of substituted PPE differs from that of the backbone conformation of the polydots formed by bare PPE. The alkyl chains appear to prevent the close packing of PPEs without side chains. While some of the coiling observed may be a result of the preparation method, the tight packing in absence of the side chains is an inherent characteristic for conjugated polymers that are assembled without side chains.[36] The comparison between the two conformations presented in Figure 3a and 3b provides a clear evidence that the side chains tune the internal conformation and, therefore, could serve as a potential design tool for polydots with specific photophysics.

The radii of gyration Rg of substituted PPE polydots in implicit poor solvents as a function of time for T = 300, 400, and 600 K are shown in Figure 4. At 300 K, after an initial small expansion in the first ns, Rg remains constant over the entire length of the simulation. Increasing the temperature to 400 K of substituted PPE polydot results in a slow increase in the instantaneous R_g over ~150 ns, after which the size of the polydots remains stable. The root mean square radius of gyration $<R_g^2>^{1/2}$ increases from ~ 26 Å at 300K to ~ 28Å for the substituted PPE polydot. For the bare PPE polydots, the increase is much larger, from ~ 18Å to ~ 24.7 Å and the chains rearrange to form a 2 nm diameter cavity. Both types of polydots become more aspherical at 400 K compared to 300 K. At 600 K, the increase in Rg is more dramatic and the chains rearrange, as shown in Figure 3c for the substituted PPE polydots. For polydots of bare PPE, the size of the cavity increases to ~ 4nm in diameter. We attribute the formation of the hollow center to stress release as the temperature is raised.

The symmetry of the polydots was quantified through calculating the three eigenvalues of the moment of inertia tensor, $\lambda_1 < \lambda_2 < \lambda_3$ for both types of polydots. For a fully spherical object, these three eigenvalues are equal.[37] The calculated ratios of the eigenvalues for substituted PPE polydots, $\lambda_3/\lambda_1 = 1.2$ and $\lambda_2/\lambda_1 = 1.1$ and for bare PPE polydots , $\lambda_3/\lambda_1 = 1.6$ and $\lambda_2/\lambda_1 = 1.2$ in both implicit poor solvent and in water at 300 K. These values are larger than 1; i.e. the polydots shape diverges from a sphere. Increasing the temperature from 300 to 400 K, λ_3/λ_1 increased from 1.2 to 1.4 for the substituted polydots and 1.6 to 2.0 for the bare polydots. These values are consistent with the visual observations in Figure 3 that the polydots become significantly more aspherical at higher temperature. The increase in asphericity with increasing temperature is consistent with the PPE chains assuming a more extended conformation within the confined state.

The radial density profiles of the polydots were calculated and the results at 300 K are shown in Figure 5 in water and in an implicit poor solvent. The density of the polydots with substituted PPEs is uniform, within the noise of the measurement. Due to the large stiffness of the backbone, the centers of the polydots with substituted PPE consist almost entirely of the flexible side chains, whereas the centers of the polydots of bare PPE are hollow. For the substituted PPE polydots, the solvent exposed outer surface is mostly comprised of the flexible side chains. As shown in Figure 5, it is notable that hardly any water molecules reside inside either of the polydot; however, at the boundary of the polydots with the solvent, a higher density of water is observed over a range of approximately 1 nm. The appearance of a broad water/polydot interface is in part due to the fact that the polydots are not perfectly spherical, and their external interface is broad, particularly without side chains.

The temperature dependence of the radial densities of the polydots from their center of mass in an implicit poor solvent is shown in Figures 6a and b for the substituted and bare PPEs respectively. At 300 K the density of the substituted PPE polydots shown in Figure 6a forms a well-defined boundary with the solvent with undulations of the order of the radius of the substituted chain. Increasing the temperature to 400 K results in a slight broadening of the interface with the solvent and broadening of the undulations. At 600 K, the density profile is smooth and broad, consistent with the expanded structure shown in Figure 3. With increasing temperature, the bare PPE polydot reorganizes, as previously shown in Figure 3b, with a hollow center. This results in a density profile with its maximum offset from the center of mass, as seen in Figure 6b.

The relaxed polydots after 300 ns at 400 K and 600 K were cooled back to 300 K. After an initial slight decrease in the size, they remained in the configuration of the elevated temperature for 300 ns. This shows that once the polydots reach their higher temperature state, they remain in that state and do not return to the low-temperature, initial quasi-spherical shape.

While the overall structure of the polydots in solution is obtained computationally by visualizing the atomic coordinates, their overall shape and their internal structure are often determined experimentally through scattering techniques in which the overall structure factor of the polydots, S(q) is measured, where q is the momentum transfer vector. Experimentally, the analysis of the scattering data is model dependent and requires further support. The correlation between results from simulations and scattering provides a powerful strategy to determine the

structure of polydots in solution. The scattering factor of the polydots was calculated using $S(q) = \frac{1}{N}\sum_{i,j=1}^{N} b_i b_j \exp\left[iq.\left(r_i - r_j\right)\right] / \frac{1}{N}\sum_{i,j=1}^{N} b_i\, b_j$ where b_i, q_i, and r_i are the scattering length for neutrons, momentum transfer vector, and the position vector of atom i, respectively.[38] Results for S(q) were averaged over 500 configurations and 500 different q vectors. S(q) as a function of q for polydots in an implicit poor solvent at different temperatures is shown in Figure 7. S(q) shows a $q^{-\alpha}$ dependence with $\alpha \sim 4$ in the intermediate q regime, characteristic for a spherical object. These simulation results capture the shape of the polydots in the low q region together with internal structural features at high q.

With increasing temperature, S(q) in the low q regime for the polydot that consist of substituted PPEs, is shifted to lower q values as expected for an object that expands, as shown in Figure 6a. At 600 K, however, the slope α at the intermediate q range changes from 4 to 2.3, consistent with the visual transition from a sphere to fused rings. Further, the peaks that correspond to the side chains and other internal dimensions broaden as expected from a more dynamic chain, which will be further discussed in the dynamics section. To compare with experimental studies and the visualization of the particle shown in Figure 3, a form factor of a fuzzy sphere[39] was used to fit S(q). The form factor for a fuzzy sphere incorporates the typical sphere scattering convoluted with a Gaussian to account for the gradual drop-off in the density of the object. While the polydots at 300 K and 400 K could be well described by a fuzzy sphere form factor, the polydot at 600 K assumed a different shape. The value of the radius of gyration for polydots at 300 K and 400 K obtained from the fits fit are 25.1 Å and 30.7 Å, respectively, which are consistent with the calculated radii of gyration. Experimental studies of polydots in water have shown the evolution of their shape from spherical to oblate as the function of temperature[40] but did not access this high-temperature regime.

For polydots comprising of bare PPEs, with increasing temperature, S(q) changes as the polydot loses its shape, as shown in Figure 7b. With increasing temperature, the slope decreases from $\alpha = 4$ to ~ 2.2, which validates the visual observation shown in Figure 3 that at higher temperatures the polydot becomes aspherical. In this case, S(q) was fitted using the fuzzy sphere form factor at 300 K. The polydot at higher temperatures were fitted to a donut-like shape of the polydot.

B. Dynamic Studies

To examine the relaxation of the polydots on different length scales, we calculated the coherent dynamic structure factor S(q,t), where q is the momentum transfer vector and t, reflecting dynamics as measured by neutron spin echo spectroscopy. [41]

$$S(q,t) = \frac{1}{N}\sum_{i,j=1}^{N} b_i b_j < \exp\left[i\boldsymbol{q}\cdot\left(\boldsymbol{r_i}(t) - \boldsymbol{r_j}(0)\right)\right] >.$$

S(q,t) was calculated using 2,000 configurations, each separated by 0.1 ns, and averaged over 500 q vectors. S(q,t)/S(q,0) for the polydot with substituted PPE chains as a function of time in water and in implicit poor solvent at 300 K are shown in Figure 8. The values of q chosen correspond to a dimension of 1–10 nm, which probes the relaxation of the polydot together with their internal motions. In order to resolve the internal dynamics S(q,t) was compared to that measured for the polydots whose translational motion was removed in the analysis. S(q,t) is nearly independent of whether the center of mass motion is arrested in water, as demonstrated in Figure 8a, indicating that the translational diffusion of the polydot is slow and the relaxation observed is due largely to internal relaxation or rigid body rotation. This finding is consistent with the measured diffusion constant D ~ 8.0 x10^{-5} nm^2/ns of the polydots or an average mean square displacement of 0.14 nm over the 40 ns time scale shown in Figure 8a. On the length scale of the polydots, hardly any relaxation occurs. At higher q values, however, S(q,t) decays, indicative of dynamic processes within the length scales and Fourier times probed. Similar results were found for the polydot in an implicit poor solvent, as shown in Figure 8b. The overall trends in S(q,t) obtained in the implicit poor solvent are similar to those obtained in the water. Comparing the diffusion constant of the polydot in water with that in the implicit poor solvent, D ~ 3.4 x10^{-6} nm^2/ns, we find that the effective damping constant of water at 300K is ~24 fs.

S(q,t) for the polydot in water and in poor solvent at 300K with the center of mass removed was analyzed to extract the effective diffusion coefficients Γ_i. A single exponential fit

the data for $q < 0.1Å^{-1}$, while for $q > 0.1Å^{-1}$ a sum of two exponentials, $S(q,t)/S(q,0) = A_1e^{-\Gamma_1 t} + (1-A_1)e^{-\Gamma_2 t}$, is required to fit the data. The values for the effective diffusion Γ_1 and Γ_2 as a function of q are presented in Figure 9 (by definition $\Gamma_1 < \Gamma_2$). The overall trend shows that the effective diffusion constant increases with increasing q, $\Gamma_1 \sim q^x$ with $x \sim 2.6$ for water and 2.2 in implicit solvent at 300K. The relaxation is slightly slower (larger Γ_i) for the polydot in water than in implicit poor solvent, presumably due to the effect of the interfacial water compared to an implicit solvent.

The dynamic structure factor in an implicit poor solvent at 300 and 400 K is shown in Figure 10. At high q values, which measure the internal motions including the side chain dynamics and backbone fluctuations, S(q,t) fully decays within the time range measured at both 300 and 400 K. However as the temperature increases, S(q,t) decays faster over the time scale measured. The values for the effective diffusion Γ_1 and Γ_2 as a function of q are presented in Figure 11 ($\Gamma_1 < \Gamma_2$). For the slowest relaxation Γ_1 the scaling exponent x decreases from 2.2 to 2.0 as the temperature is increased from 300 to 400 K. The overall internal effective diffusion increases with increasing temperature.

To separate the internal relaxation from the rigid body rotation, we also simulated the polydot in a poor solvent with the constraint that the linear and angular momenta of the entire object are both zero. S(q,t) for this case is shown in Figure 12a. S(q,t) decays very slowly, as the overall motion of the polydot has been removed. These data show that when the backbone and side chains were probed separately as shown in Figures 12b, the side chains remain dynamic, while the backbone of the confined PPE chain is glassy. For short time scales of a few picoseconds, the relaxation is due predominantly to the motion of the side chains. To further validate that the side chain motion is predominant, we measured the mean square displacement for the end C atom of the side chains; the results show that they move, on average, 1.6 nm in 1 ns, which accounts for the observed decay in S(q,t).

The S(q,t) decay pattern of the backbone shows that in the confined geometry the backbone is glassy. The autocorrelation function $\langle N(t) \bullet N(0) \rangle$, where N(t) is the normal to the plane of the aromatic ring, was then measured. While it takes only about 3 ns for the aromatic ring to rotate and become uncorrelated for an extended PPE chain,[42] under confinement the motion is significantly restricted, as shown in Figure 13. The inset shows the backbone of the

polydot, in which aromatic rings that have undergone rotation of > 180° after 300 ns are represented in red. The snapshot clearly shows that the rings are free to rotate and are distributed throughout the polydot, not just confined to the interface. The relaxation does not fit a simple exponential but can be fit using the Kohlrausch-Williams-Watt (KWW)[43] function $\langle N(t) \bullet N(0) \rangle = A \exp(-t/\tau)^{\beta}$, where β is the stretched exponential and τ is the characteristic relaxation time for motion. The fitted values of $\tau = 3.5$ μs and $\beta = 0.8$.

5. Conclusions

This study has provided for the first time an insight into the structure, stability, and dynamics of soft nanoparticles or polydots. The conformation and dynamics of the polymers within their confined geometry were probed as a function of temperature for alkyl-substituted PPE and bare PPE chains. We find that the substituting side chains strongly impact the overall conformation of the PPE polydots and affect their structure and stability. The presence of side chains results in a random pattern of the PPE backbones within the polydots in contrast to more periodic structures without the side chains. With increasing temperature, the polydots evolve from spherical to aspherical objects and, surprisingly, develop cavities in their centers. The decrease in density in the center of the polydots is more pronounced for bare PPE polydots. We attribute these conformational changes to a stress release path of the PPE, whose lowest energy conformation is extended.

The dynamic studies have shown that the backbone of the PPE within the polydot is glassy and hardly moves, while the side chains remain dynamic. The autocorrelation of the aromatic rings results in a time constant in the microsecond range, while the side chains remain dynamic in the nanosecond time range. With increasing temperature, the polydots slightly expand, and the chains become more dynamic. However, the backbone motion is hardly increased.

This study has shown that polydots are glassy soft nanoparticles whose internal conformation and dynamics are tunable by the nature of the substituents of the conjugated backbone. This understanding provides an insight into designing tools for soft polymeric nanoparticles with tunable photophysics.

Acknowledgements

The authors gratefully acknowledge financial support from NSF grant CHE 1308298. This work was made possible by advanced computational resources deployed and maintained by Clemson Computing and Information Technology. This research used resources obtained through the Advanced Scientific Computing Research (ASCR) Leadership Computing Challenge (ALCC) at the National Energy Research Scientific Computing Center (NERSC), which is supported by the Office of Science of the U.S. Department of Energy under Contract No. DEAC02-05CH11231. The research was carried out, in part, at the Center for Integrated Nanotechnologies, a U.S. Department of Energy and Office of Basic Energy Sciences user facility. Sandia National Laboratories is a multi-program laboratory managed and operated by Sandia Corporation, a wholly owned subsidiary of Lockheed Martin Corporation, for the U.S. Department of Energy's National Nuclear Security Administration under Contract No. DE-AC04-94AL85000.

* Corresponding Author, email:dperahi@g.clemson.edu

† Present Address: Oak Ridge National Laboratory, Oak Ridge, TN

References:

(1) Wu, C.; Chiu, D. T. Highly Fluorescent Semiconducting Polymer Dots for Biology and Medicine. *Angewandte Chemie-International Edition* **2013**, *52*, 3086-3109.
(2) Feng, L. H.; Zhu, C. L.; Yuan, H. X.; Liu, L. B.; Lv, F. T.; Wang, S. Conjugated polymer nanoparticles: preparation, properties, functionalization and biological applications. *Chemical Society Reviews* **2013**, *42*, 6620-6633.
(3) Tuncel, D.; Demir, H. V. Conjugated polymer nanoparticles. *Nanoscale* **2010**, *2*, 484-494.
(4) Li, S.; Shen, X.; Li, L.; Yuan, P.; Guan, Z.; Yao, S. Q.; Xu, Q.-H. Conjugated-Polymer-Based Red-Emitting Nanoparticles for Two-Photon Excitation Cell Imaging with High Contrast. *Langmuir* **2014**, *30*, 7623-7627.
(5) Li, K.; Liu, B. Polymer encapsulated conjugated polymer nanoparticles for fluorescence bioimaging. *Journal of Materials Chemistry* **2012**, *22*, 1257-1264.
(6) Pecher, J.; Mecking, S. Nanoparticles of Conjugated Polymers. *Chemical Reviews* **2010**, *110*, 6260-6279.
(7) Feng, X.; Lv, F.; Liu, L.; Tang, H.; Xing, C.; Yang, Q.; Wang, S. Conjugated Polymer Nanoparticles for Drug Delivery and Imaging. *Acs Applied Materials & Interfaces* **2010**, *2*, 2429-2435.
(8) Peng, H. S.; Chiu, D. T. Soft fluorescent nanomaterials for biological and biomedical imaging. *Chemical Society Reviews* **2015**, *44*, 4699-4722.

(9) Gezici, O.; Durmaz, I.; Guven, E. B.; Unal, O.; Ozgun, A.; Cetin-Atalay, R.; Tuncel, D. Dual functionality of conjugated polymer nanoparticles as an anticancer drug carrier and a fluorescent probe for cell imaging. *RSC Advances* **2014**, *4*, 1302-1309.
(10) Dmitriev, R. I.; Borisov, S. M.; Dussmann, H.; Sun, S. W.; Muller, B. J.; Prehn, J.; Baklaushev, V. P.; Klimant, I.; Papkovsky, D. B. Versatile Conjugated Polymer Nanoparticles for High-Resolution O-2 Imaging in Cells and 3D Tissue Models. *Acs Nano* **2015**, *9*, 5275-5288.
(11) Chamberlayne, C. F.; Lepekhina, E. A.; Saar, B. D.; Peth, K. A.; Walk, J. T.; Harbron, E. J. Functionalization of Conjugated Polymer Nanoparticles for Fluorescence Photomodulation. *Langmuir* **2014**, *30*, 14658-14669.
(12) Feng, L.; Liu, L.; Lv, F.; Bazan, G. C.; Wang, S. Preparation and Biofunctionalization of Multicolor Conjugated Polymer Nanoparticles for Imaging and Detection of Tumor Cells. *Advanced Materials* **2014**, *26*, 3926-3930.
(13) Zhang, W.; Sun, H.; Yin, S. Y.; Chang, J. J.; Li, Y. H.; Guo, X. Y.; Yuan, Z. Bright red-emitting polymer dots for specific cellular imaging. *Journal of Materials Science* **2015**, *50*, 5571-5577.
(14) Ahmed, E.; Morton, S. W.; Hammond, P. T.; Swager, T. M. Fluorescent Multiblock pi-Conjugated Polymer Nanoparticles for In Vivo Tumor Targeting. *Advanced Materials* **2013**, *25*, 4504-4510.
(15) Kurokawa, N.; Yoshikawa, H.; Hirota, N.; Hyodo, K.; Masuhara, H. Size-dependent spectroscopic properties and thermochromic behavior in poly(substituted thiophene) nanoparticles. *Chemphyschem* **2004**, *5*, 1609-1615.
(16) Schutze, F.; Krumova, M.; Mecking, S. Size Control of Spherical and Anisotropic Fluorescent Polymer Nanoparticles via Precise Rigid Molecules. *Macromolecules* **2015**, *48*, 3900-3906.
(17) Grey, J. K.; Kim, D. Y.; Norris, B. C.; Miller, W. L.; Barbara, P. F. Size-dependent spectroscopic properties of conjugated polymer nanoparticles. *Journal of Physical Chemistry B* **2006**, *110*, 25568-25572.
(18) Maskey, S.; Osti, N. C.; Perahia, D.; Grest, G. S. Internal Correlations and Stability of Polydots, Soft Conjugated Polymeric Nanoparticles. *ACS Macro Letters* **2013**, *2*, 700-704.
(19) Liu, J. W.; Mackay, M. E.; Duxbury, P. M. Nanoparticle formation by crosslinking a macromolecule. *EPL* **2008**, *84*, 46001.
(20) Beck, J. B.; Killops, K. L.; Kang, T.; Sivanandan, K.; Bayles, A.; Mackay, M. E.; Wooley, K. L.; Hawker, C. J. Facile Preparation of Nanoparticles by Intramolecular Cross-Linking of Isocyanate Functionalized Copolymers. *Macromolecules* **2009**, *42*, 5629-5635.
(21) Wu, C.; Bull, B.; Szymanski, C.; Christensen, K.; McNeill, J. Multicolor Conjugated Polymer Dots for Biological Fluorescence Imaging. *ACS Nano* **2008**, *2*, 2415-2423.
(22) Wu, C.; Szymanski, C.; Cain, Z.; McNeill, J. Conjugated polymer dots for multiphoton fluorescence imaging. *Journal of the American Chemical Society* **2007**, *129*, 12904-12905.
(23) Wu, C. F.; Szymanski, C.; McNeill, J. Preparation and encapsulation of highly fluorescent conjugated polymer nanoparticles. *Langmuir* **2006**, *22*, 2956-2960.
(24) Szymanski, C.; Wu, C. F.; Hooper, J.; Salazar, M. A.; Perdomo, A.; Dukes, A.; McNeill, J. Single molecule nanoparticles of the conjugated polymer MEH-PPV, preparation and characterization by near-field scanning optical microscopy. *Journal of Physical Chemistry B* **2005**, *109*, 8543-8546.

(25) Maskey, S.; Pierce, F.; Perahia, D.; Grest, G. S. Conformational study of a single molecule of poly para phenylene ethynylenes in dilute solutions. *Journal of Chemical Physics* **2011**, *134*, 244906.
(26) Jorgensen, W. L.; Maxwell, D. S.; TiradoRives, J. Development and testing of the OPLS all-atom force field on conformational energetics and properties of organic liquids. *Journal of the American Chemical Society* **1996**, *118*, 11225-11236.
(27) Jorgensen, W. L.; Madura, J. D.; Swenson, C. J. Optimized intermolecular potential functions for liquid hydrocarbons. *Journal of the American Chemical Society* **1984**, *106*, 6638-6646.
(28) Hockney, R. W.; Eastwood, J. W. *Computer Simulation Using Particles*; Adam Hilger-IOP: Bristol, 1988.
(29) Plimpton, S. Fast parallel algorithms for short-range molecular-dynamics. *Journal of Computational Physics* **1995**, *117*, 1-19.
(30) Schneider, T.; Stoll, E. Molecular-dynamics study of a three-dimensional one-component model for distortive phase transitions. *Phys. Rev. B* **1978**, *17*, 1302-1322.
(31) Grest, G. S.; Kremer, K. Molecular-dynamics simulation for polymers in the presence of a heat bath. *Physical Review A* **1986**, *33*, 3628-3631.
(32) Berendsen, H. J. C.; Grigera, J. R.; Straatsma, T. P. The missing term in effective pair potentials. *Journal of Physical Chemistry* **1987**, *91*, 6269-6271.
(33) Andersen, H. C. Rattle - a velocity version of the shake algorithm for molecular-dynamics calculations. *Journal of Computational Physics* **1983**, *52*, 24-34.
(34) Ryckaert, J. P.; Ciccotti, G.; Berendsen, H. J. C. Numerical-integration of cartesian equations of motion of a system with constraints - molecular-dynamics of n-alkanes. *Journal of Computational Physics* **1977**, *23*, 327-341.
(35) Murat, M.; Grest, G. S. Structure of a grafted polymer brush - a molecular-dynamics simulation. *Macromolecules* **1989**, *22*, 4054-4059.
(36) Hwang, E.; Lusker, K. L.; Garno, J. C.; Losovyj, Y.; Nesterov, E. E. Semiconducting polymer thin films by surface-confined stepwise click polymerization. *Chemical Communications* **2011**, *47*, 11990-11992.
(37) Theodorou, D. N.; Suter, U. W. Shape of unperturbed linear-polymers - polypropylene. *Macromolecules* **1985**, *18*, 1206-1214.
(38) Sorensen, C. M. Light scattering by fractal aggregates: A review. *Aerosol Science and Technology* **2001**, *35*, 648-687.
(39) Stieger, M.; Richtering, W.; Pedersen, J. S.; Lindner, P. Small-angle neutron scattering study of structural changes in temperature sensitive microgel colloids. *Journal of Chemical Physics* **2004**, *120*, 6197-6206.
(40) Osti, N. C. Neutron study of structure and dynamics of rigid polymers. PhD., Clemson University2014.
(41) Richter, D.; Monkenbusch, M.; Arbe, A.; Colmenero, J. *Neutron Spin Echo in Polymer Science*; Springer Berlin Heidelberg **2005**.
(42) Wijesinghe, S.; Maskey, S.; Perahia, D.; Grest, G. S. Accepted to Journal of Polymer Science. *Journal of Polymer Science, Part B:Polymer Physics,published online (2015)*.
(43) Williams, G.; Watts, D. C. Non-symmetrical dielectric relaxation behaviour arising from a simple empirical decay function. *Transactions of the Faraday Society* **1970**, *66*, 80-85.

Figures:

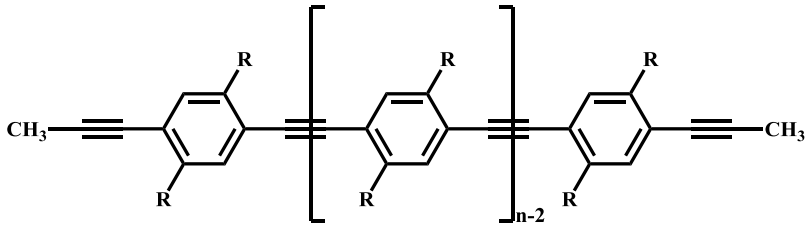

Figure 1: The chemical structure of PPE where R represents an alkyl chain. In this study, R includes ethylhexyl and H and n = 240.

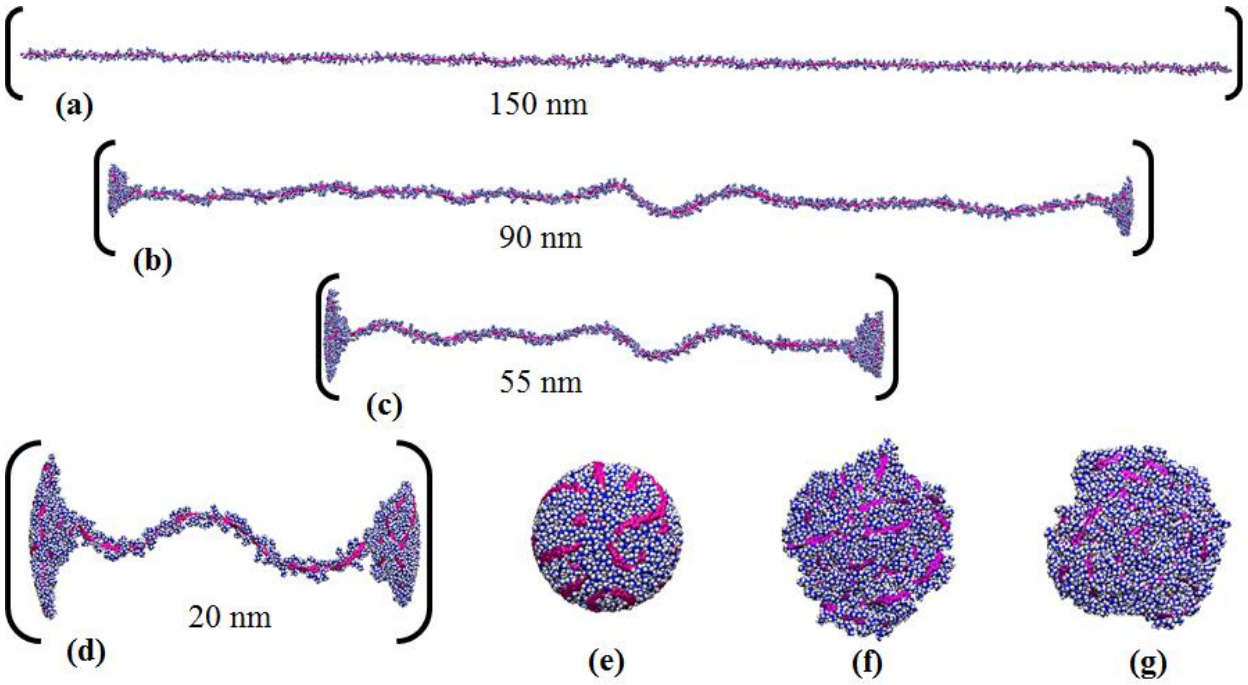

Figure 2: Sample images of diethylhexyl PPE for (a) t = 0 ns, (b) t = 0.5ns, (c) t = 0.75 ns, (d) t = 0.9 ns, (e) t = 1ns, (f) polydot in implicit poor solvent, and (g) polydot in water at 300 ns. The distances marked correspond to the dimension of the full object. For clarity, dark blue corresponds to carbon atoms on the side chains, white to hydrogen atoms on the side chains, and magenta to all atoms on the backbone.

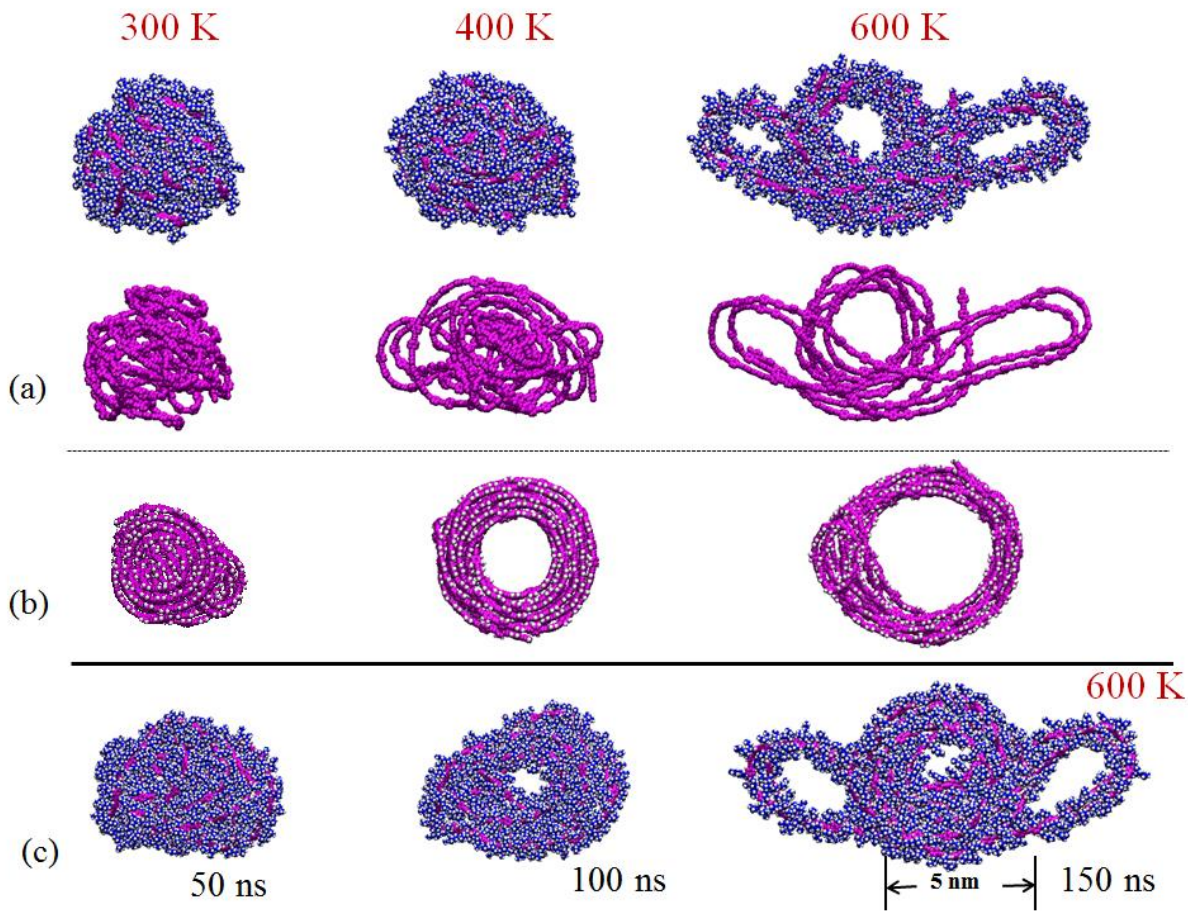

Figure 3: Sample images of (a) alkyl-substituted PPE and its backbone and (b) bare PPE in an implicit poor solvent after 300 ns. (c) Time evolution of substituted PPE polydots as a function of time at 600 K. Carbon atoms on side chains of substituted PPE polydots are marked in dark blue, hydrogen atoms in white, and backbones in magenta.

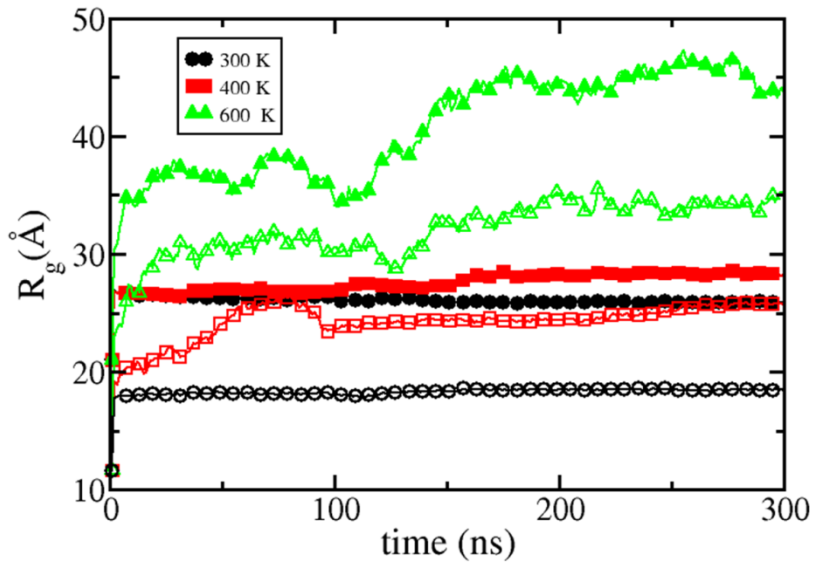

Figure 4: Radius of gyration Rg versus time for the substituted PPE polydot (solid) and polydot made of bare PPE chain (open) as a function of time at indicated temperatures.

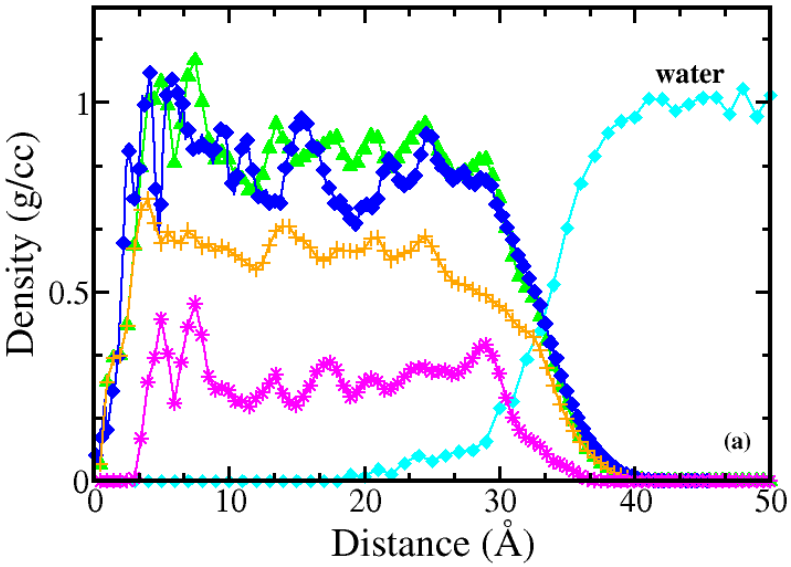

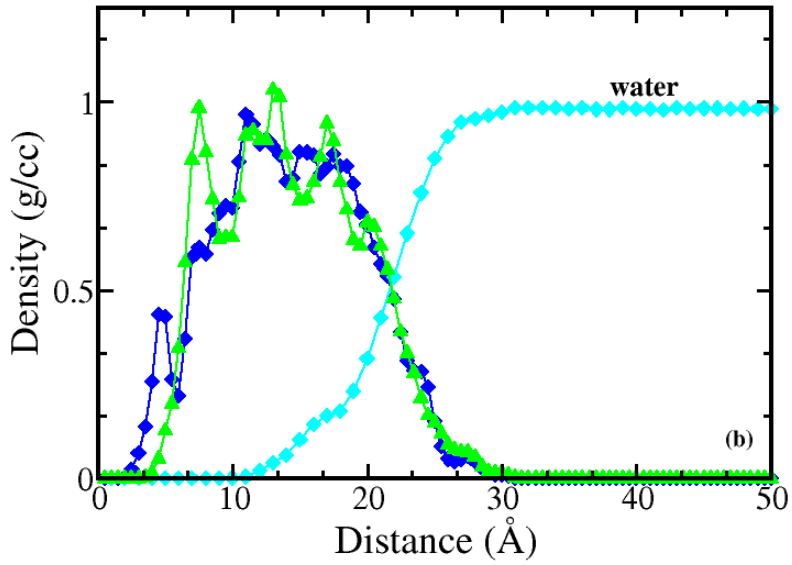

Figure 5: Radial mass density as a function of distance from the center of the polydot in water (diamonds) and in an implicit poor solvent (triangles) at T = 300 K for (a) substituted PPE polydots and (b) polydots made of bare PPE. The density of water is shown by squares. For polydots with side chains in (a), orange represents the side chains and magenta represents the backbones.

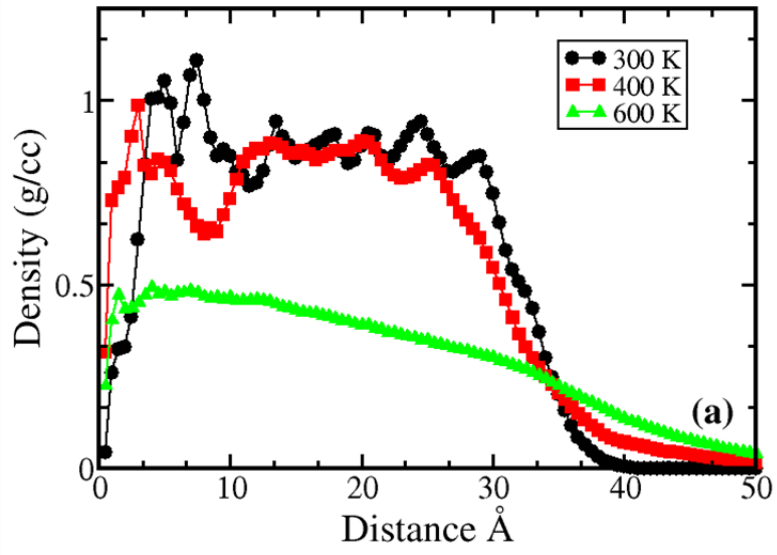

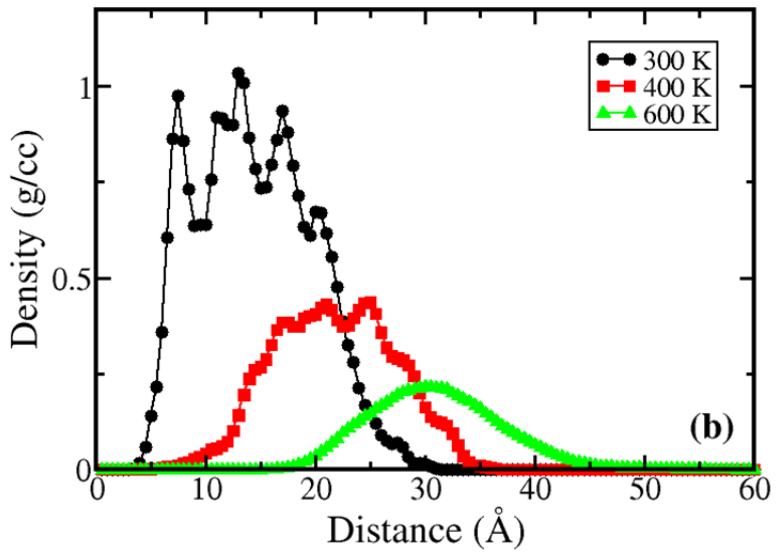

Figure 6: Radial density as a function of distance from the center of polydot for (a) substituted PPE and (b) bare PPE chains at indicated temperature.

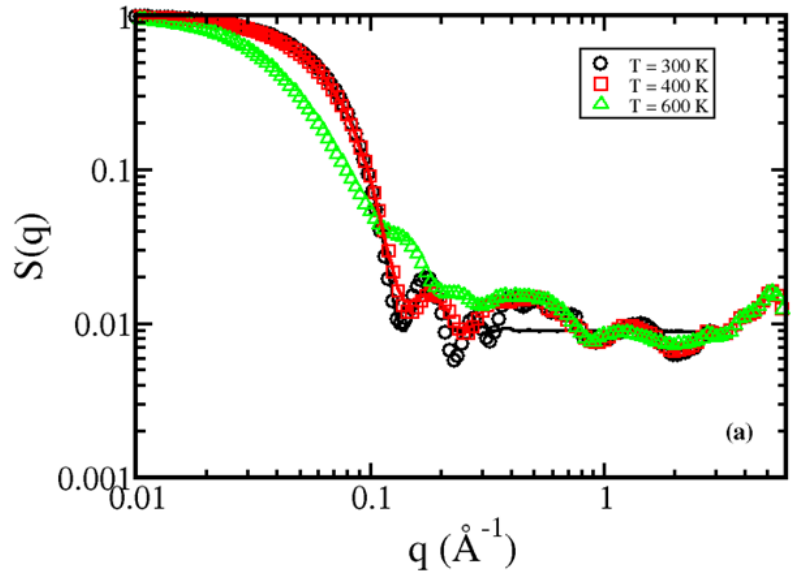

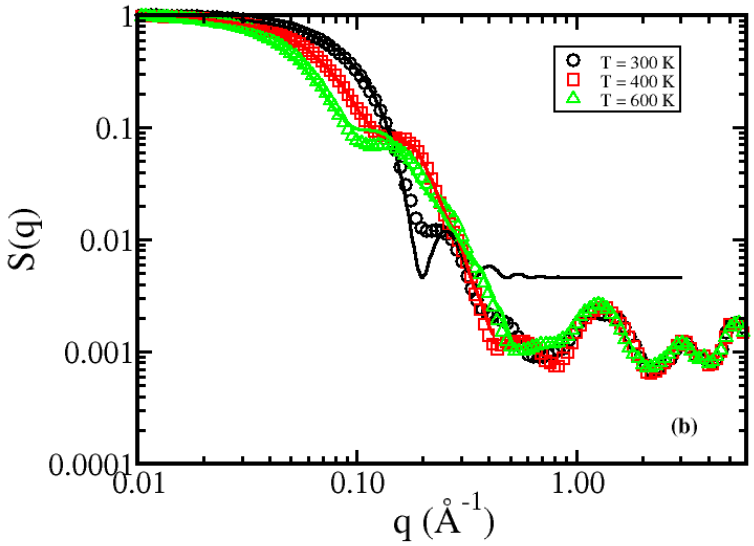

Figure 7: S(q) as the function of q for polydots with (a) substituted PPE and (b) bare PPE chains in an implicit poor solvent at the indicated temperatures. The solid line represents a fit to a fuzzy sphere model.

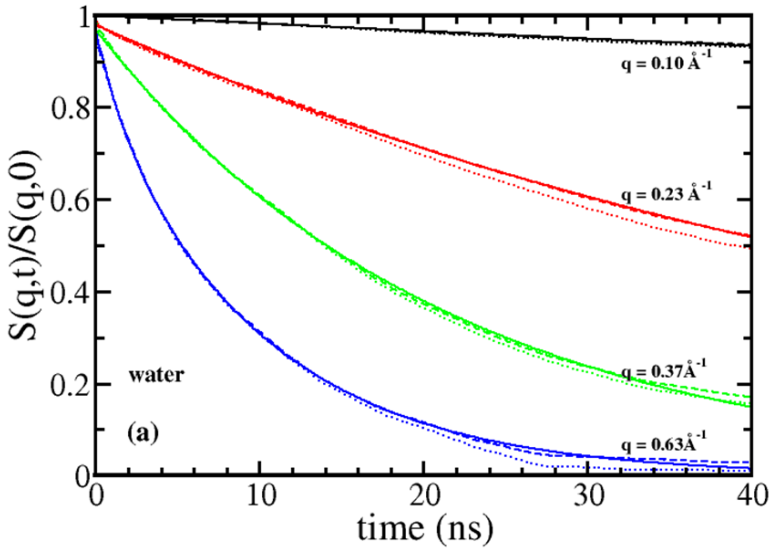

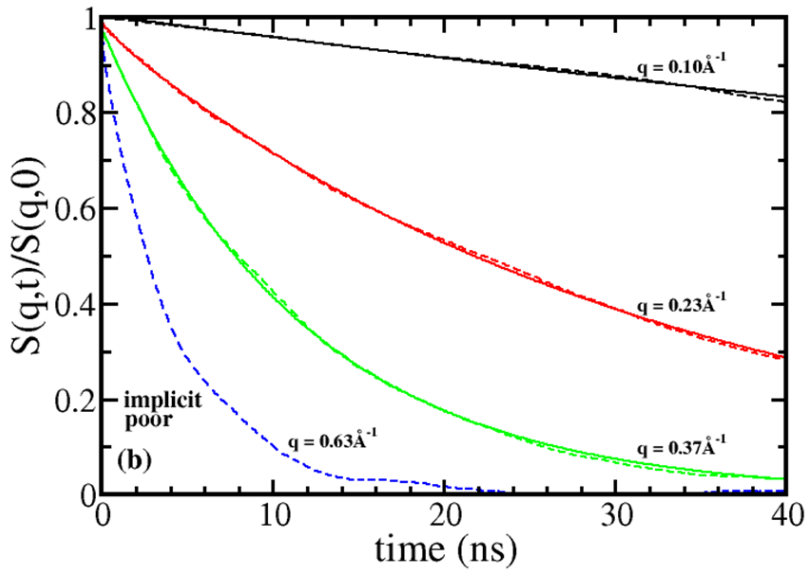

Figure 8: S(q,t)/S(q,0) as the function of time at 300 K for polydots with substituted PPE chains (a) in water and (b) in implicit poor solvent. The dotted lines represent data without the center of mass subtracted, and the dashed lines represent the data with the center of mass motion arrested. The solid line is the fit to the data with the center of mass motion removed. All the data have been fitted with single exponentials for $q < 0.1Å^{-1}$ and sum of two exponentials for $q > 0.1Å^{-1}$.

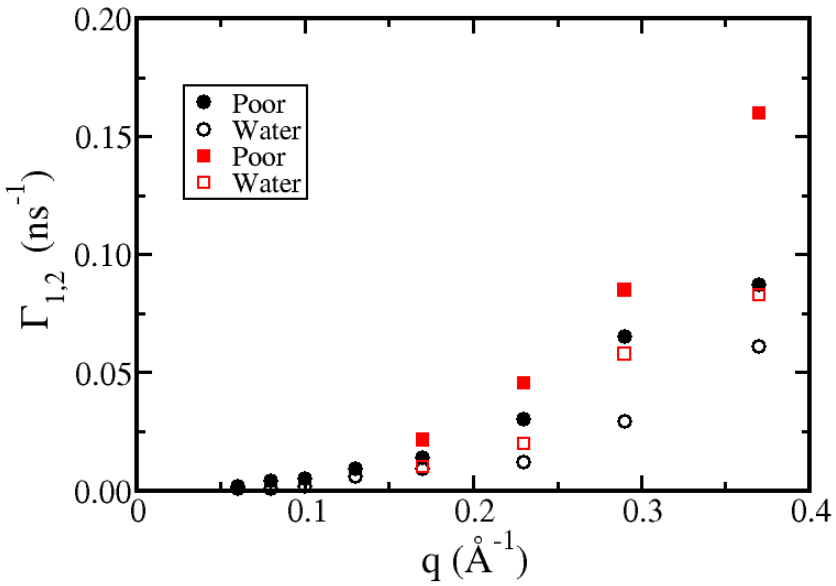

Figure 9: Γ_1 (black circles) and Γ_2 (red squares) as the function of q for polydots of substituted PPE in water (open) and implicit poor solvent (closed) at 300K.

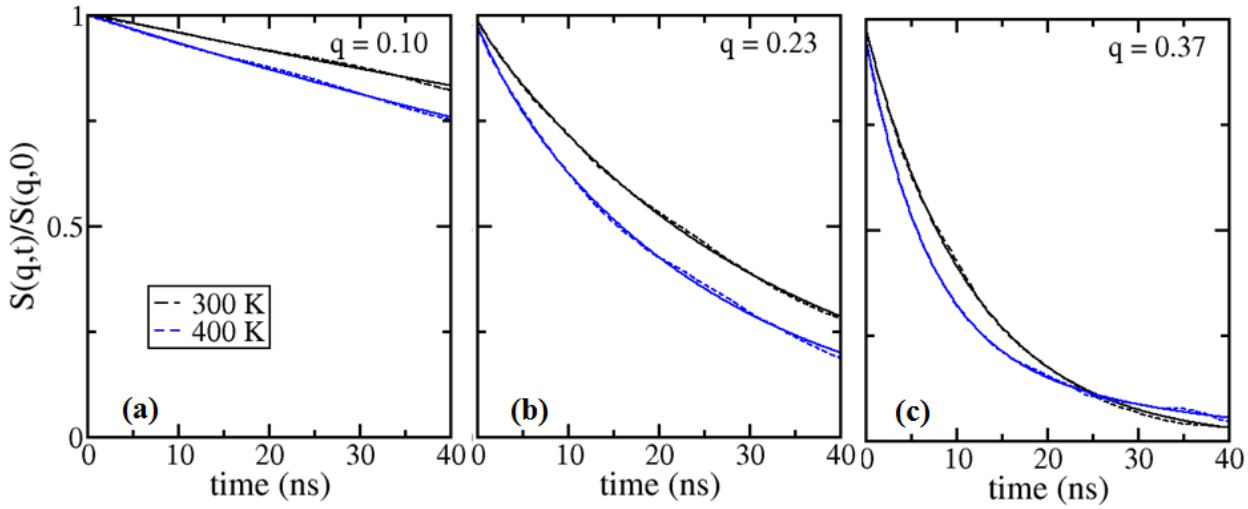

Figure 10: S(q,t)/S(q,0) as the function of time for polydots of substituted PPE in a poor solvent at different temperatures.

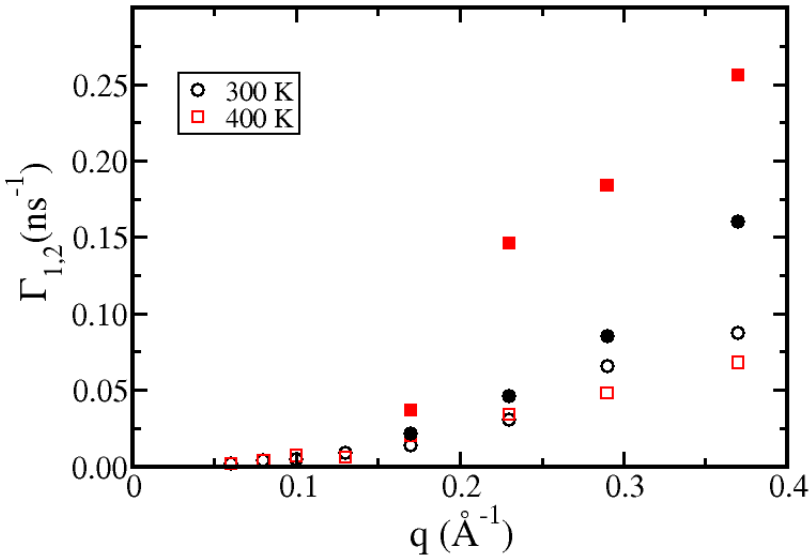

Figure 11: Γ_1 (open symbol) and Γ_2 (closed symbol) as the function of q for polydot of substituted PPE chains in an implicit poor solvent at the indicated temperatures.

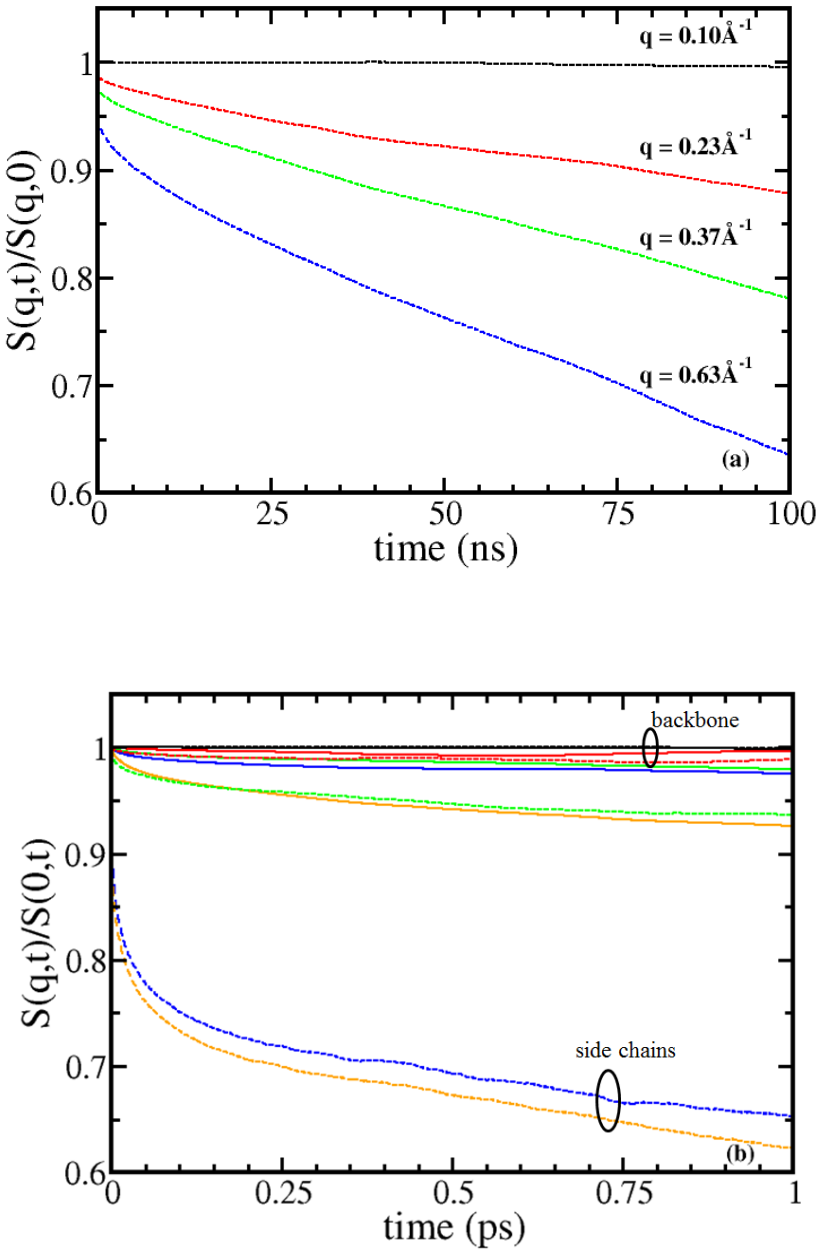

Figure 12: (a) S(q,t)/S(q,0) as the function of time for polydots of substituted PPE chains in poor solvent at 300 K with angular and linear momentum set to zero. (b) Represents S(q,t)/S(q,0) of side chains (dashed lines) and backbones (solid line) of polydots for q = 0.06 Å^{-1}(black) q = 0.10 Å^{-1} (red), q = 0.23Å^{-1} (green), q = 0.37Å^{-1} (blue) and q =0.63 Å^{-1} (orange).

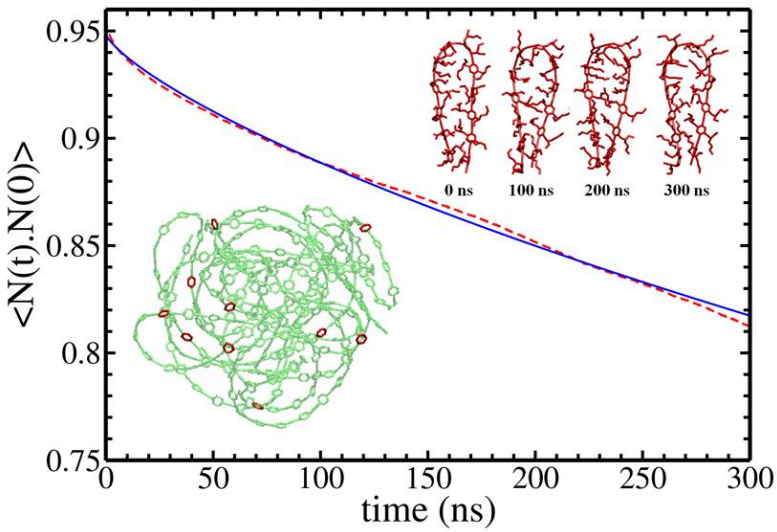

Figure 13: Autocorrelation function for aromatic rings in substituted PPE backbone of polydots in a poor solvent with linear and angular momentum arrested (red). The blue line represents the best fit to the stretched exponential. The lower inset shows the backbone of polydot where red-colored aromatic rings have rotated more than 180° after 300 ns, and the upper inset shows 12 aromatic rings of the backbone at the indicated times.

TABLE OF CONTENTS: